

Multi-modal Multi-kernel Graph Learning for Autism Prediction and Biomarker Discovery

Junbin Mao^a, Jin Liu^{a,*}, Hanhe Lin^c, Hulin Kuang^a, Shirui Pan^d and Yi Pan^{b,*}

^aThe Hunan Province Key Lab on Bioinformatics, School of Computer Science and Engineering, Central South University, Changsha 410083, China

^bThe Faculty of Computer Science and Control Engineering, Shenzhen Institute of Advanced Technology, Chinese Academy of Sciences, Shenzhen 518055, China

^cThe School of Science and Engineering, University of Dundee, DD1 4HN Dundee, United Kingdom

^dThe School of Information and Communication Technology, Griffith University, Gold Coast, QLD 4215, Australia

ARTICLE INFO

Keywords:

Multi-modal integration
Graph learning
Multi-kernel learning
Autism prediction
Biomarker discovery

ABSTRACT

Due to its complexity, graph learning-based multi-modal integration and classification is one of the most challenging obstacles for disease prediction. To effectively offset the negative impact between modalities in the process of multi-modal integration and extract heterogeneous information from graphs, we propose a novel method called MMKGL (Multi-modal Multi-Kernel Graph Learning). For the problem of negative impact between modalities, we propose a multi-modal graph embedding module to construct a multi-modal graph. Different from conventional methods that manually construct static graphs for all modalities, each modality generates a separate graph by adaptive learning, where a function graph and a supervision graph are introduced for optimization during the multi-graph fusion embedding process. We then propose a multi-kernel graph learning module to extract heterogeneous information from the multi-modal graph. The information in the multi-modal graph at different levels is aggregated by convolutional kernels with different receptive field sizes, followed by generating a cross-kernel discovery tensor for disease prediction. Our method is evaluated on the benchmark Autism Brain Imaging Data Exchange (ABIDE) dataset and outperforms the state-of-the-art methods. In addition, discriminative brain regions associated with autism are identified by our model, providing guidance for the study of autism pathology.

1. Introduction

The development of medical devices has facilitated the acquisition of multi-modal clinical data. It has been found that multi-modal data could benefit disease prediction as it contains more information than single-modal data (Mohammadi-Nejad et al., 2017) by taking advantage of the joint and supplementary information. Recently, a few approaches that aim to make use of multi-modal data for disease prediction have been proposed, including multi-modal fusion methods based on attention mechanisms (Zhu et al., 2022; Zheng et al., 2022), multi-task learning (Adeli et al., 2019; Jie et al., 2015), and nonnegative matrix decomposition (Zhou et al., 2019; Peng et al., 2022). However, these approaches rely on feature learning and do not adequately explore the structure and cross-modal relationships between modalities. As a result, how to fully exploit the knowledge of multi-modal is still a long-standing research topic.

Owing to the inherent properties of graphs (Su et al., 2020) such as information aggregation and relationship modeling, graph models provides an efficient way for integrating multi-modal information. Graph neural networks

(GNNs) have been proposed in (Welling and Kipf, 2016). Due to their advantages of joint population learning and information mining, a growing number of GNN-based studies have been proposed for disease prediction. PopGCN (Parisot et al., 2017) is the first application of graph convolutional networks to Autism and Alzheimer's disease. It combines brain imaging information and phenotypic information jointly to construct disease population graphs and perform disease prediction to distinguish normal individuals from patients. InceptionGCN (Kazi et al., 2019a) explored the impacts of the size of convolutional filters on disease prediction based on PopGCN, and tried to find the optimal convolutional filter size. MMGL (Zheng et al., 2022) used a self-attentive mechanism to learn complementary information between modalities and is used to construct disease population graphs.

Although the above studies have achieved promising results for disease prediction, there are some limitations. One of the most challenging problems is that the domain distributions of different modalities vary significantly. It leads to the fact that when multi-modal data are directly integrated, the less expressive modalities may suppress the expression of other modal data. This phenomenon is known as the inter-modal negative impact. Another major issue is that most of the existing graph convolutional network-based disease prediction methods use a size-fixed convolutional filter, which cannot well extract the heterogeneous information over the graph.

To overcome these problems and to effectively utilize multimodal data, we propose a novel framework entitled

*This work was supported in part by the National Natural Science Foundation of China under Grant 62172444 and U22A2041, in part by the Shenzhen Science and Technology Program under Grant KQTD20200820113106007, in part by the Natural Science Foundation of Hunan Province under Grant 2022JJ30753, in part by the Central South University Innovation-Driven Research Programme under Grant 2023CXQD018, and in part by the High Performance Computing Center of Central South University.

*Corresponding author

✉ liujin06@csu.edu.cn (Liu); yi.pan@siaat.ac.cn (Pan)

Multi-modal Multi-Kernel Graph Learning (MMKGL). The contributions of our work are summarized as follows:

- We propose a multi-modal graph embedding module that generates multiple graphs adaptively, where each graph corresponds to one modal data. A function graph and a supervision graph are introduced to optimize the multi-graph fusion embedding process, which effectively mitigates the negative impacts between modalities.
- We propose a multi-kernel graph learning network that extracts heterogeneous information by using convolutional kernels with different receptive field sizes. To minimize the graph noise, a relational attention mechanism (RAM) is deployed to adaptively tune the graph structure in the training process.
- The proposed framework is evaluated on the Autism Brain Imaging Data Exchange (ABIDE) dataset. The results verify the validity of our proposed framework and demonstrate its advantages over state-of-the-art methods. The code of MMKGL will be made available at the time of publication.
- Discriminative brain regions and subnetworks with discriminatory properties are discovered, giving guidance for the study of autism pathology.

2. Related Work

In this section, we mainly review automatic disease diagnosis works from multi-modal analysis and graph neural networks.

2.1. Multi-modal Analysis for Disease Prediction

Multi-modal analysis for disease prediction aims to explore complementary and specific information of modalities in a specific way and use them for disease prediction. Traditional multi-modal approaches usually concatenate multi-modal features in the original space to perform disease prediction (Ritter et al., 2015). However, such approaches cannot take full advantage of the complementary information presented in multi-modal data.

An increasing number of researchers have started to explore more intricate multi-modal approaches (Peng et al., 2022; Zhou et al., 2019; Zheng et al., 2022; Song et al., 2022; Zhang et al., 2022b; Zhu et al., 2022). Peng et al. (2022) utilized a joint non-negative matrix decomposition algorithm (GJNMFO) to identify abnormal brain regions associated with diseases by projecting three modal data into different coefficient matrices. Zhou et al. (2019) learned a latent space for multi-modal data that retains modality-specific information, and then projected the features of the latent space into the label space for prediction. Song et al. (2022) constructed a fused brain functional connectivity networks by applying different strength penalty terms for different modalities. To combine heterogeneous structural information between multi-modal states, Zhang et al. (2022b) proposed a fusion

algorithm based on graph popular regularization. Zhu et al. (2022) proposed a triple network to explore higher-order discriminative information in multi-modal while extracting complementary information from fMRI and DTI (Diffusion Tensor Imaging) using cross-attention. Zheng et al. (2022) exploited attention-based pattern-aware learning to mine complementary information between multi-modal data. Unlike the fusion at the feature level in (Zheng et al., 2022), our framework transforms multi-modal data into graphs for fusion.

2.2. Graph Neural Networks in Disease Prediction

Graph neural networks (GNNs) (Welling and Kipf, 2016) provide a practical solution for exploiting potential information from different modalities. Most early studies on GNNs-based disease prediction rely on either single modal data (Kazi et al., 2019a) or manually constructed static graphs (Parisot et al., 2017). For the former, it lacks rich multi-modal information. For the latter, it brings a lot of noise to the graph.

Some GNNs methods that use multi-modal data and adaptive graph learning have been proposed in recent years (Huang and Chung, 2022; Cosmo et al., 2020; Zheng et al., 2022; Ji and Zhang, 2022; Li et al., 2022; Zhang et al., 2022a). Huang and Chung (2022) constructed a pairwise encoder between subjects from phenotypic information to learn the adjacency matrix weights. Cosmo et al. (2020) learned optimal graphs for downstream classification of diseases based on dynamic and local graph pruning. Ji and Zhang (2022) learned graph hash functions based on phenotypic information and then used them to transform deep features into hash codes to predict the classes of brain networks. Li et al. (2022) proposed an edge-based graph path convolution algorithm that aggregates information from different paths and the algorithm is suitable for dense graphs like brain function networks. Gürbüz and Rekik (2021) proposed the multi-view graph normalizer network (MGN-Net) to normalize and integrate a set of multi-view biological networks into a single connective template. Chaari et al. (2022) introduce a multi-graph integration and classifier network (MICNet) and applies to gender fingerprinting. Zhang et al. (2022a) designed a local-to-global graph neural network to explore the global relationships between individuals and the local connections between brain regions. Zheng et al. (2022) used the complementary and shared information between multi-modalities to learn the structure of graphs through an adaptive learning mechanism of graphs. Different from the two-layer graph convolutional network used in (Zheng et al., 2022), our multi-kernel graph learning network contains different convolutional kernels that can efficiently extract the heterogeneous information of a graph.

3. METHODOLOGY

3.1. Overview

For multi-modal data, the inputs of the m -th modality consists of features $\mathbf{X}^m = \{x_1^m, x_2^m, \dots, x_N^m\}$ of N subjects.

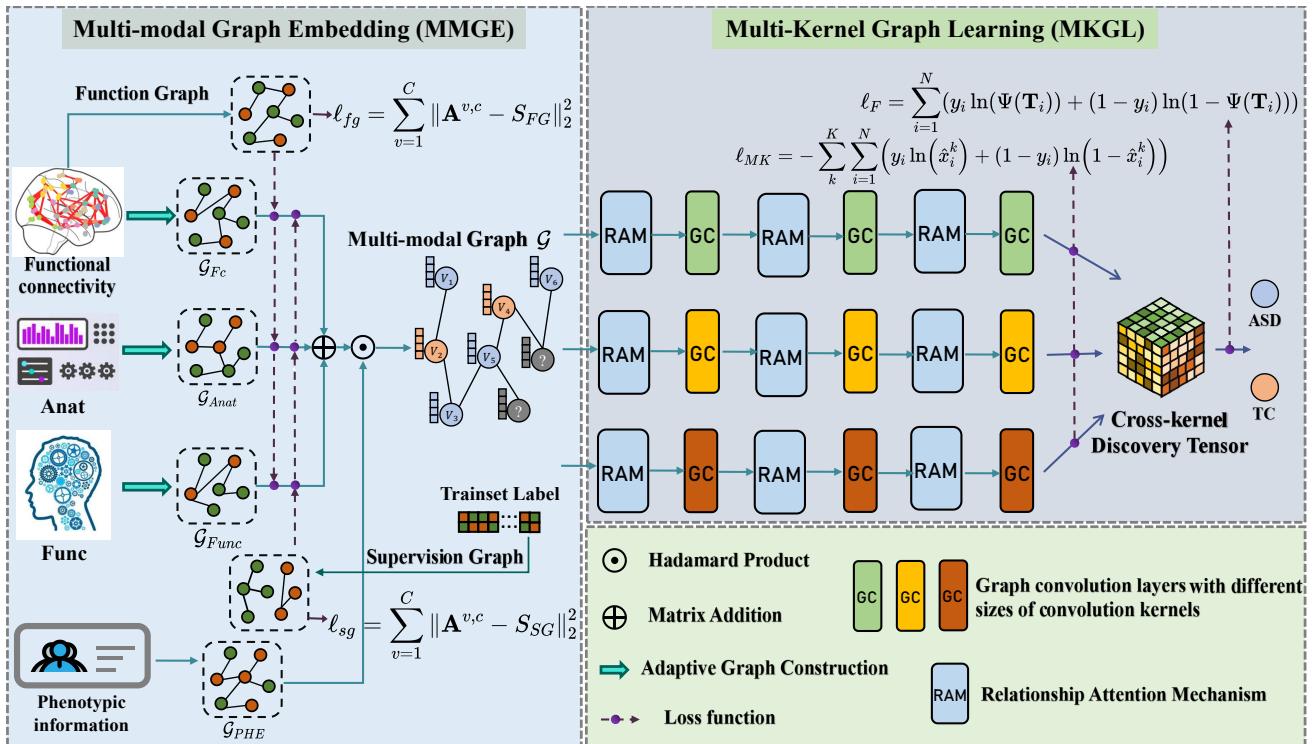


Figure 1: Overview of the architecture of our framework. **Multi-modal graph embedding:** Multiple modal graphs \mathcal{G}_{FC} , \mathcal{G}_{Anat} , \mathcal{G}_{Func} are generated by adaptive graph construction and then are fused into a Multi-modal graph \mathcal{G} . The function graph S_{FG} and supervision graph S_{SG} are introduced in the fusion process for optimization. **Multi-kernel graph learning:** The heterogeneous information of the Multi-modal graph \mathcal{G} is extracted using a graph convolutional network with different convolutional kernel sizes and fused by generating a cross-kernel discovery tensor \mathbf{T} for predicting autism spectrum disorder (ASD) and typical control (TC). In addition, relationship attention mechanism (RAM) is used to adjust the weights of the adjacency matrix \mathbf{A} .

For the multi-modal features of each subject $x_i \in \mathbf{X}$, there is an associated label $y_i \in \mathbf{Y}$. The task is defined on the dataset with \mathbf{X} as the input and \mathbf{Y} as the prediction target. Given a graph $\mathcal{G} = (\mathcal{V}, \mathcal{E}, \mathbf{X})$, \mathcal{V} is a set of nodes and \mathcal{E} is a set of edges (e.g. $e_{ij} \in \mathcal{E}$ if and only if the distance between v_i and v_j is below a threshold), where $v_i \in \mathcal{V}$ denotes the i -th node which represents a subject in autism prediction. $e_{ij} = \langle v_i, v_j \rangle$ describes the relationship between subject i and j . In addition, the adjacency matrix $\mathbf{A} \in \mathbb{R}^{N \times N}$ is derived from the set of edges \mathcal{E} , where \mathbf{A}_{ij} corresponds to the weights of e_{ij} .

As shown in Fig. 1, our proposed framework mainly consists of two modules, i.e., Multi-modal Graph Embedding and Multi-Kernel Graph Learning.

Multi-modal Graph Embedding constructs a separate graph for each modality by adaptive graph construction. Then, multi-graph fusion is performed under the supervision of a function graph S_{FG} and a supervision graph S_{SG} . Finally, phenotypic information is embedded into the fused graph to generate a multi-modal graph \mathcal{G} .

Multi-Kernel Graph Learning acquires heterogeneous information of the multi-modal graph \mathcal{G} through convolutional kernels of different sizes. Among them, relational attention mechanism is proposed to adjust the weights of individual relations in the multi-modal graph \mathcal{G} with the self-adaptation. Finally, a cross-kernel discovery tensor is gen-

erated by fusing the heterogeneous information and used for autism prediction.

3.2. Data acquisition and Preprocessing

We validate our framework on the publicly available Autism Brain Imaging Data Exchange (ABIDE) (Di Martino et al., 2014) dataset. It collects data from 17 international sites and contains neuroimaging and phenotypic data of 1,112 subjects. In this study, followed by the same imaging criteria in (Abraham et al., 2017), 871 subjects were selected, where 403 are with ASD and 468 are with typical control (TC). To ensure equitability and reproducibility, the fMRI data was processed by using the Configurable Pipeline for the Analysis of Connectomes (CPAC) from the Preprocessed Connectomes Project (PCP) (Craddock et al., 2013). The preprocessed functional images were registered to a standard anatomical space (MNI152). Subsequently, the average time series of brain regions were extracted according to the automatic anatomical atlas (AAL).

Four modalities were selected for this study. 1) *Brain functional connectivity* (FC): Calculated from time series of brain regions based on Pearson’s correlation coefficient. 2) *Phenotype information* (PHE): Including age, gender, site, and scale information. 3) *Automated anatomical quality assessment metrics* (Anat): Reflecting indicators such as smoothness of Voxels, percentage of Artifact Voxels, and

signal to noise ratio. 4) *Automated functional quality assessment metrics* (Func): Reflecting indicators such as entropy focus criterion, standardized DVARS, and mean distance to median volume. Anat and Func are proven to be effective in disease prediction (Zheng et al., 2022).

3.3. Multi-modal Graph Embedding

3.3.1. Graph Construction

We divide the four modalities into two categories based on their properties: 1) Continuous Data \mathbf{X}^c : FC, Anat, and Func. 2) Discrete Data \mathbf{X}^d : PHE.

For continuous features \mathbf{X}^c , we calculate cosine similarity between pairs of subjects and maps onto the $[0, 1]$ interval by rescaling to construct an adjacency matrix $\mathbf{A}^{v,c}$ of v -th modality, where v includes FC, Anat, and Func. The similarity between subject i and subject j is defined as:

$$\mathbf{A}_{ij}^{v,c} = \frac{(x_i^v \Theta^v)^\top x_j^v \Theta^v}{2 \|x_i^v \Theta^v\| \|x_j^v \Theta^v\|} + 0.5, \quad (1)$$

where x_i^v is the feature of v -th modality of i -th subject. In order to allow the features of each modality to learn adaptively during the composition, the projection transformation of the subspace is applied to the features before estimating the cosine similarity. Θ^v is the projection matrix (Implemented by a full connectivity layer) of the v -th modal.

For discrete features \mathbf{X}^d , i.e., PHE, we calculate the correlation between pairs of subjects using attribute matching. We construct an adjacency matrix $\mathbf{A}^{v,d}$ for v -th modality. The similarity between subject i and subject j is estimated as:

$$\mathbf{A}_{ij}^{v,d} = \sum_{t=1}^T \phi_t(P_i^{v,t}, P_j^{v,t}), \quad (2)$$

where ϕ_t denotes the attribute matching function used in discrete features for variables of type t , P is the discrete feature of its corresponding type. For example, if P is gender with a binary type feature, we let ϕ to be $\{e_{ij} = 1 \mid \text{if } P_i = P_j\}$. Similarly, when P is age data, we let ϕ to be $\{e_{ij} = 1 \mid \text{if } |P_i - P_j| < \theta\}$.

In addition, we introduce a supervision graph \mathbf{S}_{SG} and a function graph \mathbf{S}_{FG} for optimization during the multi-graph fusion embedding, defined as:

$$\mathbf{S}_{SG}^{ij} = \begin{cases} 1, & y_i = y_j \quad (\text{train labels}) \\ 0, & y_i \neq y_j \quad (\text{train labels}) \end{cases}, \quad (3)$$

$$\mathbf{S}_{FG}^{ij} = \exp\left(-\frac{(\mathbf{x}_i^{FC} - \mathbf{x}_j^{FC})^2}{2\sigma^2}\right), \quad (4)$$

where σ is Gaussian kernel, \mathbf{x}_i^{FC} and \mathbf{x}_j^{FC} are FC features of subject i and j . The reason for choosing FC is that it has the best representational ability.

3.3.2. Graph Integration

In order to learn towards the optimal graph for \mathbf{A}^c , we design a loss function to optimize the learning of graph structure. The reason for constructing \mathbf{S}_{SG} is that GNNs are able to classify unknown nodes quite simply if given a fully labeled graph (optimal graph). The loss is defined as follows:

$$\ell_{sg} = \sum_{v=1}^C \|\mathbf{A}^{v,c} - \mathbf{S}_{SG}\|_2^2, \quad (5)$$

where \mathbf{S}_{SG} is the supervision graph. We supervise the construction of the modal graph by \mathbf{S}_{SG} with the expectation that the transformation ability of the projection matrix of Θ will have good generalization ability.

Meanwhile, to prevent the overfitting problem caused by the supervision graph \mathbf{S}_{SG} , we introduce a function graph \mathbf{S}_{FG} constructed by the modal feature with the best expressiveness. Function graph \mathbf{S}_{FG} supervise the generation of validation and test set nodes as a way to enhance the generalization of the model, defined as follows:

$$\ell_{fg} = \sum_{v=1}^C \|\mathbf{A}^{v,c} - \mathbf{S}_{FG}\|_2^2. \quad (6)$$

Finally, the objective function of Multi-modal Graph Embedding can be expressed as the following equation:

$$\mathcal{L}_{MMGE} = \ell_{sg} + \ell_{fg}. \quad (7)$$

Using the loss function \mathcal{L}_{MMGE} , we can optimize the generation and fusion embedding of multiple modal graphs well to obtain a multi-modal graph \mathcal{G} that is close to the optimal graph and use it for autism prediction.

The adjacency matrix \mathbf{A} of the multi-modal graph \mathcal{G} can be obtained from the adjacency matrices $\mathbf{A}^{v,c}$ and $\mathbf{A}^{v,d}$, which is given by:

$$\mathbf{A} = \frac{1}{C} \sum_{v=1}^C \mathbf{A}^{v,c} \odot \frac{1}{D} \sum_{v=1}^D \mathbf{A}^{v,d}, \quad (8)$$

where C and D are the number of continuous and discrete modalities, respectively. \odot is matrix Hadamard product. In our experiment, C and D are 3 and 1, respectively.

3.4. Multi-Kernel Graph Learning

The multi-modal graph \mathcal{G} consists of edges \mathcal{E} (relationships) and nodes \mathcal{V} (subjects). To characterize the connections between nodes and nodes in the multi-modal graph \mathcal{G} , a better choice is the regularized Laplacian matrix: $L = I - D^{-\frac{1}{2}} \mathbf{A} D^{-\frac{1}{2}}$, where \mathbf{A} is the multi-modal graph adjacency matrix, D is the degree matrix of the nodes, and I is a identity matrix. Since L is a real symmetric positive semidefinite matrix, we can use the matrix decomposition as $L = U \Lambda U^\top$,

Algorithm 1 Multi-modal Multi-Kernel Graph Learning

Input: Multi-modal data \mathbf{X} , continuous-type modal \mathbf{X}^c , discrete-type modal \mathbf{X}^d , prediction target \mathbf{Y} .

MMGE:

1: Initialize adaptive graph construction weights with Θ^c .

2: **for** each continuous-type modal $\mathbf{X}^v \in \mathbf{X}^c$ in parallel **do**

3: $\mathbf{A}^{v,c} \leftarrow \cos(\mathbf{X}^v \Theta^v)$ Eq. (1)

4: **end for**

5: **for** each discrete-type modal $\mathbf{X}^v \in \mathbf{X}^d$ in parallel **do**

6: $\mathbf{A}^{v,d} \leftarrow \sum_{t=1}^T \phi_t(P_i^{v,t}, P_j^{v,t})$ Eq. (2)

7: **end for**

8: Generate adjacency matrix \mathbf{A}

9: $\mathbf{A} \leftarrow \frac{1}{C} \sum_{v=1}^C \mathbf{A}^{v,c} \odot \frac{1}{D} \sum_{v=1}^D \mathbf{A}^{v,d}$ Eq. (8)

MKGL:

1: Initialize multiple graph learning network with $\Phi(\mathcal{G})$.

2: Initialize fully connected network $\Psi(\cdot)$.

3: $\hat{\mathbf{A}} \leftarrow \text{RAM}(\mathbf{A})$ Eq. (22)

4: **for** graph learning network $\Phi_k(\mathcal{G}) \in \Phi(\mathcal{G})$ in parallel **do**

5: $\hat{\mathbf{x}}^k \leftarrow \Phi_k(\mathbf{X} * \hat{\mathbf{A}})$ Eq. (13)

6: **end for**

7: Generate cross-kernel discovery tensor

8: $\mathbf{T} \leftarrow \prod_{k=1}^K \hat{\mathbf{x}}^{(k)}, k = 1, 2, \dots, K$ Eq. (15)

9: $\hat{\mathbf{Y}} \leftarrow \Psi(\text{Flatten}(\mathbf{T}))$ Eq. (16)

Output: $\hat{\mathbf{Y}}$

where U is a matrix composed of eigenvectors and Λ is a matrix composed of eigenvalues. For the node features \mathbf{X} (\mathbf{X}^{FC} is replaced by \mathbf{X} for simplicity of writing) and the adjacency matrix \mathbf{A} , we can obtain the representation of the graph convolution $\Phi(\mathcal{G})$ on the multi-modal graph \mathcal{G} :

$$\Phi(\mathcal{G}) = \Phi(\mathbf{X} * \mathbf{A}) = U \mathbf{A}_\theta U^T \mathbf{X}, \quad (9)$$

where $\mathbf{A}_\theta = \text{diag}(U^T \mathbf{A})$. To reduce calculation costs $O(N^2)$, Chebyshev graph convolution uses Chebyshev polynomials to approximate the spectral graph convolution. In the field of polynomial function approximation, Chebyshev polynomials are usually preferred due to their numerical stability and computational efficiency. Introducing the polynomial, let $\mathbf{A}_\theta = \sum_{i=0}^k \theta_i \Lambda^i, \theta \in \mathbf{R}^k$, so that the following equation is obtained:

$$\Phi(\mathcal{G}) = \Phi(\mathbf{X} * \mathbf{A}) = U \sum_{i=0}^k \theta_i \Lambda^i U^T \mathbf{X}. \quad (10)$$

Then by shifting the eigenvector U right into the summation equation $\sum_{i=0}^k \theta_i \Lambda^i U^T \mathbf{X}$ and passing the equation $L = U \Lambda U^T$, we can obtain the following equation:

$$\Phi(\mathcal{G}) = \Phi(\mathbf{X} * \mathbf{A}) = \sum_{i=0}^k \theta_i L^i \mathbf{X}, \quad (11)$$

where k is the order of the Chebyshev polynomial. $T_k(L) = 2LT_{k-1}(L) - T_{k-2}(L)$ is the Chebyshev polynomial defined recursively with $T_0(L) = 1$ and $T_1(L) = L$. Bringing it into Eq. (11) shows that:

$$\Phi(\mathcal{G}) = \Phi(\mathbf{X} * \mathbf{A}) = \sum_{i=0}^k \theta_i T_i(\tilde{L}) \mathbf{X}, \quad (12)$$

where $\tilde{L} = \frac{2L}{\lambda_{\max}} - I$, \tilde{L} is the rescaled graph Laplace operator. Similar to convolutional neural networks, the polynomial $T_k(\tilde{L})$ is a K -order domain aggregator that integrates the information of neighboring nodes at K steps from the central node.

According to the above derivation, the forward propagation form of the Chebyshev convolutional layer can be obtained:

$$\Phi_k(\mathcal{G}) = \Phi_k(\mathbf{X} * \mathbf{A}) = \sum_{i=0}^k T_i(\tilde{L}) \mathbf{X} \mathbf{W}_i, \quad (13)$$

where $\Phi_k(\mathcal{G}) \in \mathbb{R}^{N \times H'}$ represents the Chebyshev convolution of order k on the graph \mathcal{G} . $\mathbf{X} \in \mathbb{R}^{N \times H}$, where H is the feature dimension of input \mathbf{X} . $\mathbf{W}_i \in \mathbb{R}^{H \times H'}$, where H' is the output dimension of the fully connected layer \mathbf{W}_i .

3.4.1. Cross-kernel Discovery Tensor

With the information aggregation of multiple Chebyshev graph convolutional networks of different orders, we obtain the heterogeneous information of the input features \mathbf{X} on the graph \mathcal{G} . Before \mathbf{X} is input to the feature fusion module, we train each Chebyshev network by the cross-entropy loss function so that its output $\Phi_k(\mathcal{G})$ has a better representation before fusion. The loss function is shown as follows:

$$\ell_{MK} = - \sum_k \sum_{i=1}^N (y_i \ln(\hat{x}_i^k) + (1 - y_i) \ln(1 - \hat{x}_i^k)), \quad (14)$$

where \hat{x}_i^k is the output of a Chebyshev convolutional network of order k . Next, we use the fusion module to fuse the outputs of multiple Chebyshev convolutional networks. Fusion module is designed to learn the cross-correlation of higher-level intra-view and heterogeneous graph information in the label space. For the predicting probability distribution $(\hat{x}_i^{(k)}, k = \{1, 2, \dots, K\})$ of the i -th sample from the output of different Chebyshev convolutional networks Φ_k , we construct a Cross-Kernel Discovery Tensor (CKDT) $\mathbf{T}_i \in \mathbb{R}^{t \times K}$, where t is the number of classes. The formula is defined as follows:

$$\mathbf{T}_i = \prod_{k=1}^K \hat{x}_i^{(k)}, k = 1, 2, \dots, K \quad (15)$$

\mathbf{T}_i is then flattened to a 1-dimensional vector and the final prediction is made using the fully connected network $\Psi(\cdot)$, where the loss function is written as:

$$\ell_F = \sum_{i=1}^N (y_i \ln(\Psi(\mathbf{T}_i)) + (1 - y_i) \ln(1 - \Psi(\mathbf{T}_i))). \quad (16)$$

The objective function of Multi-Kernel Graph Learning can be expressed as the following equation:

$$\mathcal{L}_{MKGL} = \ell_{MK} + \ell_F. \quad (17)$$

Eventually we optimize our model using \mathcal{L}_{MMGE} and \mathcal{L}_{MKGL} until convergence, and the total loss function can be expressed as follows:

$$\mathcal{L} = \lambda_1 \mathcal{L}_{MMGE} + \lambda_2 \mathcal{L}_{MKGL} \quad (18)$$

where λ_1 and λ_2 are the weight parameters of the corresponding loss functions, respectively. Algorithm 1 details the procedure of our proposed MMKGL framework.

3.4.2. Relational Attention Mechanism

To reduce the noise of the multi-modal graph \mathcal{G} , we propose a Relational Attention Mechanism (RAM) to learn specific information between subjects. Specifically, we first filter the more valuable individual relationships from the multi-modal graph \mathcal{G} by threshold. A less noisy adjacency matrix $\hat{\mathbf{A}}$ is generated by the learnable parameters ψ , i.e., edges of the same class are weighted more and those across class are weighted less. The RAM can be expressed as:

$$R_{ij} = \xi(\psi\theta_i, \psi\theta_j), \quad (19)$$

where θ_i, θ_j are the subject's FC feature embedding, and R_{ij} is the learned relational attention score, which represents the informational relational reference importance of subject j to subject i . Learned parameter $\psi \in \mathbb{R}^{F \times Z}$, where F is the dimension of feature θ and Z is the dimension of the hidden unit, $\xi \in \mathbb{R}^{2Z \times 1}$ is the relational attention operator. To make the relational attention scores easily comparable across subjects, we normalize all choices for subject j using the *Softmax* function:

$$\hat{\mathbf{A}}_{ij} = \text{Softmax}(R_{ij}) = \frac{\exp(R_{ij})}{\sum_{e \in N_i} \exp(R_{ie})}, \quad (20)$$

where $\hat{\mathbf{A}}_{ij}$ is the normalized relational attention weight and N_i is the neighboring node with which subject i is associated.

In this study, the relational attention operator ξ is a single-layer feedforward neural network. The information relationship between subjects can be expressed as:

$$\hat{\mathbf{A}}_{ij} = \frac{\exp(\sigma(\xi^T [\psi\theta_i \sqcup \psi\theta_j]))}{\sum_{e \in N_i} \exp(\sigma(\xi^T [\psi\theta_i \sqcup \psi\theta_e]))}, \quad (21)$$

where T denotes the transpose, \sqcup denotes the concatenate operation. σ is the activation function, in our experiment, we use *LeakyRelu* and the negative input slope ($s = 0.2$) of the nonlinear activation function σ . To ensure the stability of the relationship between pairs of subjects, we extend the RAM to be multi-head, which can be expressed as:

$$\hat{\mathbf{A}}_{ij} = \frac{1}{Q} \sum_{q=1}^Q \frac{\exp(\sigma(\xi_q^T [\psi_q\theta_i \sqcup \psi_q\theta_j]))}{\sum_{e \in N_i} \exp(\sigma(\xi_q^T [\psi_q\theta_i \sqcup \psi_q\theta_e]))}, \quad (22)$$

where Q is the number of heads in the multi-head RAM, ξ_q is the relational attention operator of the q -th head, and ψ_q is the learnable weight parameter of the q -th head.

4. EXPERIMENTAL RESULTS AND ANALYSIS

4.1. Experimental Settings

For a fair comparison, we performed a K-fold ($K=5$) cross-validation experiment on the ABIDE dataset. To be more specific, the dataset was split into 5 non-overlapping subsets. Each time we left one for test, and the rest for training and validation. In the training process, the model that performs best on the validation set was taken and evaluated on the test set. We repeated it 10 times, and the average performance was reported.

Four widely used metrics were applied to evaluate the performance, including accuracy (ACC), area under the curve (AUC), sensitivity (SEN), and specificity (SPE). In our experiment, hyper-parameters λ_1 and λ_2 were set to 1 empirically.

4.2. Comparison with previous work

We compare our approach with state-of-the-art (SOTA) methods, including PopGCN (Parisot et al., 2017), InceptionGCN (Kazi et al., 2019a), MultiGCN (Kazi et al., 2019c), LSTMGCN (Kazi et al., 2019b), LG-GNN (Zhang et al., 2022a), EVGCN (Huang and Chung, 2022), LGL (Cosmo et al., 2020), and MMGL (Zheng et al., 2022). Among them, both PopGCN and InceptionGCN are early disease prediction studies based on single modal data and manual construction of static graphs. MultiGCN, LSTMGCN, LG-GNN, EVGCN, LGL, and MMGL are SOTA works that make use of multi-modal data for disease prediction. Moreover, EVGCN, LGL, and MMGL are dynamic in constructing graphs.

The experimental results are shown in Table 1. As can be seen, approaches that use multi-modal generally outperform those use single modal. The average performance of the multi-modal approaches (82.72%) is 11.48% higher than the average performance of the single modal approach (71.24%). Furthermore, the performance of the methods that use dynamic graphs, i.e., EVGCN, LGL, and MMGL, has a large performance improvement over the methods that use static graphs. This confirms the advantage of dynamic graphs over static graphs, i.e., sacrificing a negligible amount of training

Table 1

The performance comparison of SOTA methods for ASD/TC classification.

Method	ACC (%)	AUC (%)	SEN (%)	SPE (%)	Modal Type	Graph Type
PopGCN (Parisot et al., 2017)	69.80 ± 3.35	70.32 ± 3.90	73.35 ± 7.74	80.27 ± 6.48	Single	Static
MultiGCN (Kazi et al., 2019c)	69.24 ± 5.90	70.04 ± 4.22	70.93 ± 4.68	74.33 ± 6.07	Multiple	Static
InceptionGCN (Kazi et al., 2019a)	72.69 ± 2.37	72.81 ± 1.94	80.29 ± 5.10	74.41 ± 6.22	Single	Static
LSTMGCN (Kazi et al., 2019b)	74.92 ± 7.74	74.71 ± 7.92	78.57 ± 11.6	78.87 ± 7.79	Multiple	Static
LG-GNN (Zhang et al., 2022a)	81.75 ± 1.10	85.22 ± 1.01	83.22 ± 1.84	82.96 ± 0.94	Multiple	Static
EVGCN (Huang and Chung, 2022)	85.90 ± 4.47	84.72 ± 4.27	88.23 ± 7.18	79.90 ± 7.37	Multiple	Dynamic
LGL (Cosmo et al., 2020)	86.40 ± 1.63	85.88 ± 1.75	86.31 ± 4.52	88.42 ± 3.04	Multiple	Dynamic
MMGL (Zheng et al., 2022)	89.77 ± 2.72	89.81 ± 2.56	90.32 ± 4.21	89.30 ± 6.04	Multiple	Dynamic
MMKGL	91.08 ± 0.59	91.01 ± 0.63	91.97 ± 0.64	90.05 ± 1.37	Multiple	Dynamic

Table 2

The performance of Modal Ablation of MMGE on MMKGL.

Method	Modal				MKGL	ACC (%)	AUC (%)	SEN (%)	SPE (%)
	PHE	Anat	Func	FC					
Backbone (Single Modal)	✓					52.99 ± 0.96	51.86 ± 0.97	67.13 ± 2.35	36.58 ± 2.62
		✓				53.75 ± 1.61	52.18 ± 1.64	73.49 ± 3.41	31.07 ± 4.11
			✓			54.17 ± 0.64	52.08 ± 0.74	79.91 ± 3.80	24.25 ± 4.51
				✓		75.07 ± 0.87	74.75 ± 0.88	78.98 ± 1.47	70.51 ± 1.78
MMKGL (Multi-modal)				✓	✓	77.76 ± 2.13	77.55 ± 2.15	81.15 ± 1.60	73.95 ± 3.31
	✓			✓	✓	81.81 ± 1.52	81.41 ± 1.49	86.30 ± 2.47	76.52 ± 2.38
	✓		✓	✓	✓	87.87 ± 0.63	87.58 ± 0.72	90.67 ± 0.91	84.48 ± 2.06
	✓	✓		✓	✓	88.47 ± 0.96	88.36 ± 0.93	90.86 ± 1.91	85.85 ± 1.28
	✓	✓	✓	✓	✓	91.08 ± 0.59	91.01 ± 0.63	91.97 ± 0.64	90.05 ± 1.37

time in exchange for model performance as well as learnability.

Among the approaches that construct graphs dynamically, the MMGL method outperforms the EVGCN and LGL methods. One possible reason is that MMGL employs cross-modal attention mechanism, which helps to capture valuable multi-modal complementary information. In contrast, our method outperforms MMGL in all four metrics. Compared to the traditional dynamic graph construction methods, our method uses multi-modal graph embedding to construct dynamic graphs, which alleviates the problem of negative effects between modal fusion. The supervision graph S_{SG} and function graph S_{FG} are also used to optimize the graph fusion process. In light of this, our dynamic graph method outperforms the SOTA methods.

4.3. Ablation Study

4.3.1. Effect of MMGE on MMKGL

To evaluate the effectiveness of different modalities, we separately input four modalities FC, Anat, Func, and PHE into the two-layer graph convolutional network (backbone). As shown in Table 2, all four modalities demonstrate their effectiveness for autism prediction, with FC exhibiting the strongest representation ability and achieving an accuracy of 75.07%, the highest among the four modalities.

Next, we evaluate the performance of modal combinations on the basis of MMKGL. We replace the backbone with MKGL and add other modalities incrementally, with FC as the primary modality. As shown in Table 2, the accuracy of MKGL+FC is 77.76%, which represents a 2.69% improvement over the backbone's accuracy (75.07%). Considering that Anat and Func are imaging information, while PHE belongs to clinical phenotype information, we first incorporate PHE into MKGL+FC, resulting in a performance of 81.81%. This indicates that PHE can effectively complement FC and improve the prediction performance of the model. We subsequently add Anat and Func to MKGL+FC+PHE, and the performance of MKGL+FC+PHE+Anat and MKGL+FC+PHE+Func reaches 88.47% and 87.87%, respectively. This suggests that Anat and Func can synergize well with the FC+PHE modality. The four modalities (FC+Func+Anat+PHE) demonstrate a higher accuracy of 91.08% than the three modalities, indicating that FC, Func, Anat, and PHE can be effectively integrated through MMGE.

4.3.2. Effect of MKGL on MMKGL

To validate the effectiveness of Multi-Kernel Graph Learning (MKGL) module, we fix the MMGE module and investigate the contribution of different components of

Table 3

The performance of Module Ablation of MKGL on MMKGL.

Method	MMGE	MKGL			ACC (%)	AUC (%)	SEN (%)	SPE (%)
		GCN	RAM	CKDT				
MMKGL	✓	✓			80.61 ± 1.24	80.66 ± 1.23	79.94 ± 2.12	81.39 ± 1.99
	✓	✓		✓	81.13 ± 1.12	81.15 ± 1.17	80.79 ± 1.90	81.51 ± 2.73
	✓	✓	✓		89.45 ± 0.79	89.37 ± 0.78	90.47 ± 1.32	88.26 ± 1.16
	✓	✓	✓	✓	91.08 ± 0.59	91.01 ± 0.63	91.97 ± 0.64	90.05 ± 1.37

MKGL.

- (1) GCN: It uses the graph convolution network only.
- (2) GCN + CKDT: It adds the CKDT to GCN.
- (3) GCN + RAM: It integrates the RAM to GCN.
- (4) MKGL: it combines both RAM and CKDT with GCN, i.e., GCN+RAM+CKDT.

The experimental results are shown in Table 3. It can be observed that the accuracy of using GCN alone is 80.61%. By separately adding CKDT and RAM to GCN, the accuracy of GCN+CKDT and GCN+RAM improve to 81.13% and 89.45%, respectively. It indicates that RAM and CKDT effectively utilize the multi-modal graph \mathcal{G} generated by MMGE to extract discriminative information for autism prediction. The accuracy of GCN+RAM+CKDT (MKGL) is 91.08%, which validates the effectiveness of MKGL. Using MKGL, our model is improved by 10.47%, which shows the promising ability to combine GCN, RAM, and CKDT.

4.3.3. Effect of Feature Fusion Method

To verify the effectiveness of the feature fusion method in CKDT, we replaced it with feature concatenation (Concat), feature addition (Add), feature weighting (Weight), and feature averaging (Avg). For feature weighting, we obtain the optimal expression by assigning different weights to the multi-modal features.

The experimental results are shown in Fig. 2. In terms of accuracy ranking, the performance of the fusion methods from high to low is Ours, Add, Concat, Avg, and Weight. Unexpectedly, the performance of the feature weighting fusion method is the worst, even lower than that of Avg. This may be due to the model learning inappropriate modality weights, which leads to relatively poor performance. According to previous research, the feature weighting fusion method generally performs well in these traditional feature fusion methods. It is worth noting that our fusion module outperforms traditional methods on all evaluation metrics. This indicates that the fusion method in CKDT can effectively integrate heterogeneous information on the graph.

4.3.4. Multiple Convolutional Kernel Combinations Analysis

To investigate the influence of convolutional kernel size on the model, we evaluate the performance of single convolutional kernels separately using a single graph convolutional network (MMGE+RAM). K is the convolution kernel receptive field size, in our experiment, $K =$

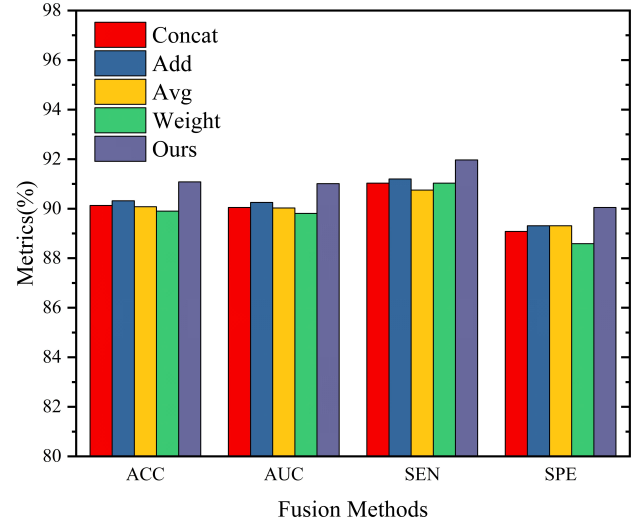


Figure 2: Performance comparison of feature fusion method in multi-kernel graph learning and traditional methods.

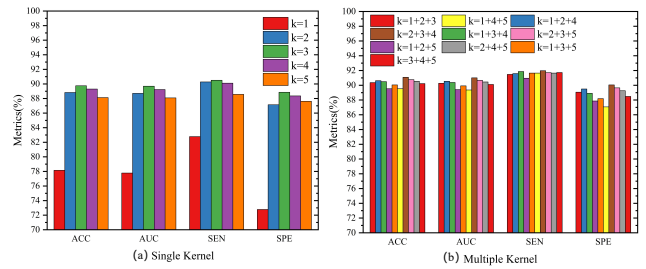


Figure 3: (a) Performance comparison of single convolutional kernel receptive field size. (b) Performance comparison of multiple combinations of convolutional kernels with different receptive field sizes.

$\{x \mid x \in N, 1 \leq x \leq 5\}$. Subsequently, we test a combination (e.g., 1+2+3, 2+3+4,...) of three randomly selected convolutional kernels from the K convolutional kernels.

The experimental results are shown in Fig. 3(a). As can be seen from, the performance of the model shows a trend of increasing and then decreasing with the increase of the receptive field K . The model performance reaches the maximum when $K=3$. Too small convolutional kernel size, i.e., $K=1$, cannot effectively extract information from the multi-modal graph \mathcal{G} , and too large convolutional kernels, e.g., $K=5$, causes an oversmoothing effect. As can be seen from

Fig. 3(b), model achieves the best performance among all combinations when the convolutional kernel combination is $K=2+3+4$. This also confirms the conclusion obtained in Fig. 3(a), i.e., the closer the convolution kernel size K is to 3, the better the performance.

4.4. Train Set Ratio Analysis

It is well known that one challenge in the field of deep learning in medicine is the lack of training data. In this context, we explore the performance of the model with a smaller data set. In the normal case, we usually use the traditional data partitioning approach, i.e., we divide the dataset into training, validation, and test sets in the ratio of 60%, 20%, and 20%, respectively.

As shown in Fig. 4, we set the training set ratio from 10% to 60%, and compare our method with MMGL and PopGCN with the same training set ratio, it is obvious that our method performs much better than the other two methods in the same ratio. Compared with MMGL and PopGCN that fluctuate largely when training set ratio increases from 30% to 60%, our method shows a smooth and stable increase. It is worth mentioning that in the lowest 10% percentage, our method works much better than MMGL and PopGCN, which indicates that our method is well suited for the domain with small data volume.

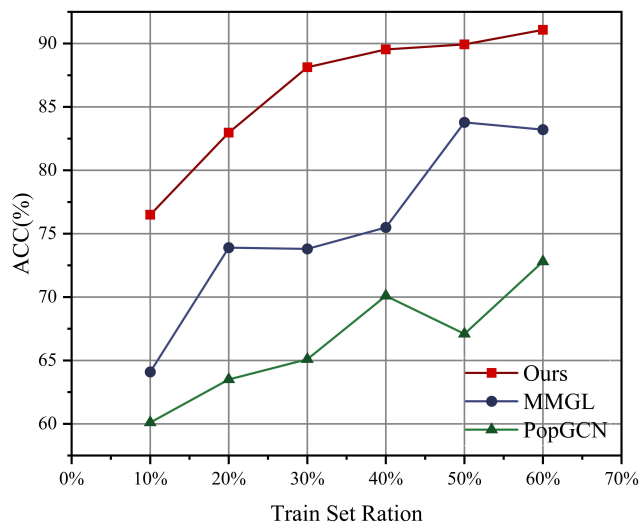


Figure 4: Accuracy comparison of multiple methods with different training set ratios.

5. Discussions

In this section, we analyze the brain regions and their constituent subnetworks that are of significant discriminatory for autism diagnosis in our model. Specifically, we use a gradient-based approach (Selvaraju et al., 2017) to present FC self-attentive weighting coefficients from the model for all subjects and to obtain the average attentional level of these FCs. Notably, we used the automatic anatomical labeling (AAL) atlas and select the top K functional connections that are most discriminatory, respectively. The top 10

and top 20 most discriminating functional connections, standardized by their weight scores, are shown in Fig. 5.

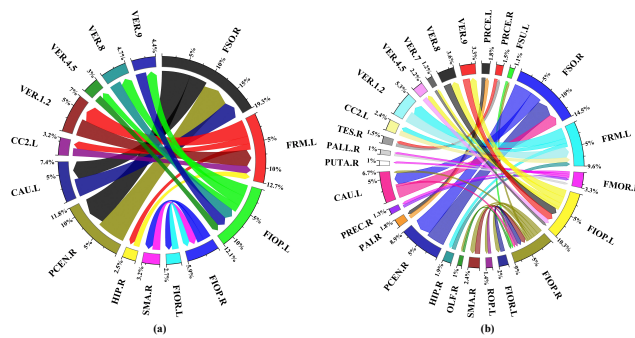


Figure 5: The figure shows the most discriminative functional connections extracted from the model weights by the gradient-based approach. The thickness of the connections represent their weights. (a) Top 10 discriminative brain functional connectivities. (b) Top 20 discriminative brain functional connectivities.

5.1. Discriminative Brain Regions

As shown in Table 4, the discriminative brain areas that distinguish autism from healthy controls included the following: Frontal Area) FSO.R, FRML.L, FIOR.P, FMOR.R. Motorium) CAUL. Sensorium) PCEN.R. Cerebellum) VER.1.2, VER.4.5, VER.8, VER.9, CC2.L. There are also some important brain areas that have a relatively small weighting, but still contribute to the diagnosis of autism, such as FIOR.L, SMA.R, HIP.R, PAIR, PRCE.L, PRCE.R. Below we discuss the role of the discriminative brain regions that we find in the pathogenesis pattern of autism of previous studies.

In a study of related literature, it was found that in the frontal orbit (FSO.R, FIOR.L), patients with asd respond to mildly aversive visual and auditory stimuli (Green et al., 2015). There are abnormalities in the morphological structure of the ossicle (FIOP) in patients with autism and normal people, and there is a correlation with social barriers. ASD's palpebral activity is relatively calm (Yamasaki et al., 2010). Frontal middle gyrus (FRML.L) gene expression in ASD is different from normal (Crider et al., 2014). The volume of the caudate nucleus is enlarged in medication-naive subjects with autism (Langen et al., 2007). The strength of connectivity within and between different functional subregions of the precentral gyrus (PRCE) is associated with the diagnosis of ASD and the severity of ASD features (Samson et al., 2012). The postcentral gyrus (PCEN) is responsible for somatosensory sensation. The postcentral gyrus cortical thickness and gray matter concentration are reduced in autistic subjects, and research has determined that the postcentral gyrus is a key brain area for ASD (Fatemi et al., 2018). Cerebellar worms have been implicated in the regulation of limbic functions, including mood, sensory reactivity, and salience detection. Association study between posterior earthworm and mesocerebellar cortex suggests cerebellum

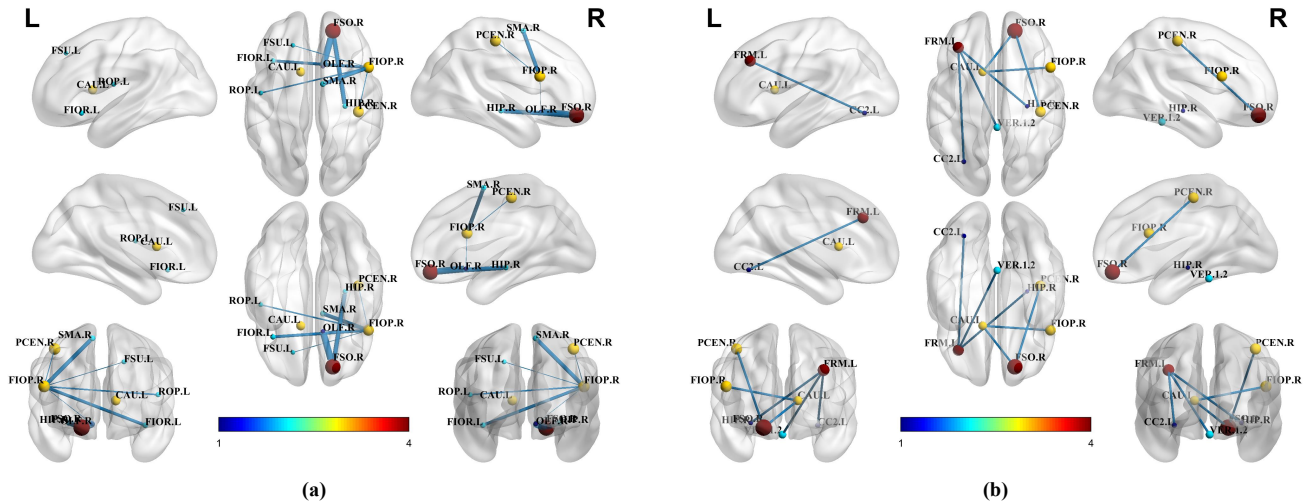


Figure 6: Visualization of the brain network composed of the top discriminative brain functional connectivities. Each figure contains views from different layouts (sagittal, axial, coronal). The color bars represent the weights of the brain regions and the thickness of the connections represent their weights. (a) Discriminative subnetworks with FIO.P.R as the center of functional connectivity. (b) Discriminative subnetworks with FSO.R and FRM.L as the center of the functional connectivity.

Table 4

The ROIs selected for the most discriminative functional connection and its normalized weight score.

ID	ROI	Anatomical Region	FC-10 Weight	FC-20 Weight
1	PRCE.L	Precentral_L	-	1.76%
2	PRCE.R	Precentral_R	-	1.53%
3	FSU.L	Frontal_Sup_L	-	1.06%
6	FSO.R	Frontal_Sup_Orb_R	19.26%	14.51%
7	FRM.L	Frontal_Mid_L	12.72%	9.58%
11	FIO.P.L	Frontal_Inf_Oper_L	12.09%	10.32%
12	FIO.P.R	Frontal_Inf_Oper_R	5.93%	8.99%
15	FIO.R.L	Frontal_Inf_Orb_L	2.71%	2.04%
17	ROP.L	Rolandic_Oper_L	-	1.40%
20	SMA.R	Supp_Motor_Area_R	3.22%	2.43%
22	OLF.R	Olfactory_R	-	0.96%
26	FMOR.R	Frontal_Mid_Orb_R	-	3.31%
38	HIP.R	Hippocampus_R	2.49%	1.87%
58	PCEN.R	Postcentral_R	11.84%	8.92%
62	PAI.R	Parietal_Inf_R	-	1.76%
68	PREC.R	Precuneus_R	-	1.28%
71	CAU.L	Caudate_L	7.42%	6.69%
74	PUTA.R	Putamen_R	-	1.02%
76	PALL.R	Pallidum_R	-	1.01%
82	TES.R	Temporal_Sup_R	-	1.53%
93	CC2.L	Cerebellum_Crus2_L	3.20%	2.41%
109	VER.1.2	Vermis_1_2	7.03%	5.30%
111	VER.4.5	Vermis_4_5	2.98%	2.25%
113	VER.7	Vermis_7	-	1.21%
114	VER.8	Vermis_8	4.74%	3.57%
115	VER.9	Vermis_9	4.37%	3.29%

plays key role in autism (Fatemi et al., 2012).

5.2. Discriminative subnetworks

We construct 2 subnetworks, as shown in Fig. 6(b). They are the subnetwork FPCF and FCVH. FPCF connects PCEN.R, CAU.L, and FIO.P.R with the brain area FSO.R as the core. According to the research of Green et al. (2015), the blood oxygen signals of the amygdala and the frontal eye

(FSO.R) in adolescents with ASD showed significant correlation changes under sensory stimulation. The amygdala and caudate nucleus (CAU.L) are directly connected in the brain. In the subnetwork we found in FPCF, CAU.L and FSO.R are connected. This may suggest that CAU.L provides a bridge for the connection between the amygdala and FSO.R. According to Glerean et al. (2016), CAU.L is clearly connected to PCEN.R in the Ventro-temporal limbic (VTL) subnetwork that differs most between the ASD and normal groups. At the same time, in VTL, CAU.L also has a certain connection with the amygdala.

The subnetwork FCVH connects CC2.L, VER.1.2, and HIP.R with the brain region FRM.L as the core. Numerous studies from neurocognitive and neuroimaging have shown that FRM is associated with the pathophysiology of ASD (Barendse et al., 2013). In addition, there is bisexual dimorphism in the middle frontal gyrus (Goldstein et al., 2001), which may be why men are four times more likely to develop autism than women. According to research by Fatemi et al. (2012), neuropathological abnormalities in autism were found in the cerebellum (CC2.L). In the subnetwork FCVH, both FRM.L and HIP.R are related to memory, and FRM.L is mainly responsible for short-term memory.

According to Table 4, there is an abnormal phenomenon, that is, the weight of the brain region FIO.P.R has increased by 3.06%. This shows that on the basis of FC-10, most of the newly added functional connections in FC-20 are related to FIO.P.R. In this regard, we use FIO.P.R as the core to visualize the brain regions (FSU.L, ROP.L, SMA.R, OLF.R, HIP.R, CAU.L, FSO.R) connected to it. The results are shown in Fig. 6(a). According to the study by Yamasaki et al. (2010), impaired social skills in autistic patients are associated with reduced gray matter volume at the FIO.P site. ROP.L has also been shown to be associated with autism in the subnet-

work AUD discovered by [Glerean et al. \(2016\)](#). ([Carper and Courchesne, 2005](#)) found that the FSU.L region of autism patients was significantly enlarged compared with controls. [Enticott et al. \(2009\)](#), identified SMA.R as a possible source of motor dysfunction in autism by examining motor-related potentials (MRPs).

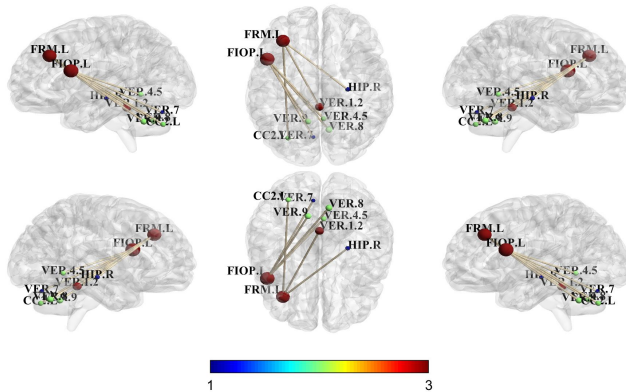


Figure 7: Discriminative subnetwork of the cerebellum and the vermis.

As shown in Fig. 5(a), the brain regions related to the cerebellum account for a larger proportion. We visualize the brain regions of the cerebellum (CC2.L, VER.1.2, VER.4.5, VER.7, VER.8, VER.9) and their connected FIOPL, FRML. The results are as follows shown in Fig. 7. As the central part of the cerebellum, vermis (VER) has the functions of regulating muscle tone, maintaining the balance of the body, and coordinating movements. [Stanfield et al. \(2008\)](#) concluded that the area of lobules I-V and VI-VII of the vermis are reduced in individuals with autism compared to controls. Loss of Purkinje cells in the posterior vermis and cerebellar intermediate cortex is the most consistent neuropathology in post-mortem dissection studies of the brains of individuals with autism ([Webb et al., 2009](#)). For more information on the pathological mechanism of the cerebellum in autism, please refer to ([Fatemi et al., 2012](#)).

6. Conclusion

In this study, we propose multi-modal multi-kernel graph learning for autism prediction and biomarker discovery. Our proposed multi-modal graph embedding is well suited to alleviate the problem of negative effects between modalities. In addition, our proposed multi-kernel graph learning network is capable of extracting heterogeneous information from multi-modal graphs for autism prediction and biomarker discovery. Finally, we find some important brain regions and subnetworks with important discriminatory properties for autism by a gradient-based approach. These findings provide important guidance for the study of autism pathological mechanisms.

References

Abraham, A., Milham, M.P., Di Martino, A., Craddock, R.C., Samaras, D., Thirion, B., Varoquaux, G., 2017. Deriving reproducible biomarkers

from multi-site resting-state data: An autism-based example. *NeuroImage* 147, 736–745.

- Adeli, E., Meng, Y., Li, G., Lin, W., Shen, D., 2019. Multi-task prediction of infant cognitive scores from longitudinal incomplete neuroimaging data. *NeuroImage* 185, 783–792.
- Barendse, E.M., Hendriks, M.P., Jansen, J.F., Backes, W.H., Hofman, P.A., Thoonen, G., Kessels, R.P., Aldenkamp, A.P., 2013. Working memory deficits in high-functioning adolescents with autism spectrum disorders: neuropsychological and neuroimaging correlates. *Journal of Neurodevelopmental Disorders* 5, 1–11.
- Carper, R.A., Courchesne, E., 2005. Localized enlargement of the frontal cortex in early autism. *Biological Psychiatry* 57, 126–133.
- Chaari, N., Gharsallaoui, M.A., Akdag, H.C., Rekik, I., 2022. Multigraph classification using learnable integration network with application to gender fingerprinting. *Neural Networks* 151, 250–263.
- Cosmo, L., Kazi, A., Ahmadi, S.A., Navab, N., Bronstein, M., 2020. Latent-graph learning for disease prediction, in: *International Conference on Medical Image Computing and Computer-assisted Intervention*, Springer. pp. 643–653.
- Craddock, C., Benhajali, Y., Chu, C., Chouinard, F., Evans, A., Jakab, A., Khundrakpam, B.S., Lewis, J.D., Li, Q., Milham, M., et al., 2013. The neuro bureau preprocessing initiative: open sharing of preprocessed neuroimaging data and derivatives. *Frontiers in Neuroinformatics* 7, 27.
- Crider, A., Thakkar, R., Ahmed, A.O., Pillai, A., 2014. Dysregulation of estrogen receptor beta ($er\beta$), aromatase ($cyp19a1$), and er co-activators in the middle frontal gyrus of autism spectrum disorder subjects. *Molecular Autism* 5, 1–10.
- Di Martino, A., Yan, C.G., Li, Q., Denio, E., Castellanos, F.X., Alaerts, K., Anderson, J.S., Assaf, M., Bookheimer, S.Y., Dapretto, M., et al., 2014. The autism brain imaging data exchange: towards a large-scale evaluation of the intrinsic brain architecture in autism. *Molecular Psychiatry* 19, 659–667.
- Enticott, P.G., Bradshaw, J.L., Ianssek, R., Tonge, B.J., Rinehart, N.J., 2009. Electrophysiological signs of supplementary-motor-area deficits in high-functioning autism but not asperger syndrome: an examination of internally cued movement-related potentials. *Developmental Medicine & Child Neurology* 51, 787–791.
- Fatemi, S.H., Aldinger, K.A., Ashwood, P., Bauman, M.L., Blaha, C.D., Blatt, G.J., Chauhan, A., Chauhan, V., Dager, S.R., Dickson, P.E., et al., 2012. Consensus paper: pathological role of the cerebellum in autism. *The Cerebellum* 11, 777–807.
- Fatemi, S.H., Wong, D.F., Brašić, J.R., Kuwabara, H., Mathur, A., Folsom, T.D., Jacob, S., Realmuto, G.M., Pardo, J.V., Lee, S., 2018. Metabotropic glutamate receptor 5 tracer [^{18}F]-fpeb displays increased binding potential in postcentral gyrus and cerebellum of male individuals with autism: A pilot pet study. *Cerebellum & Ataxias* 5, 1–8.
- Glerean, E., Pan, R.K., Salmi, J., Kujala, R., Lahnakoski, J.M., Roine, U., Nummenmaa, L., Leppämäki, S., Nieminen-von Wendt, T., Tani, P., et al., 2016. Reorganization of functionally connected brain subnetworks in high-functioning autism. *Human Brain Mapping* 37, 1066–1079.
- Goldstein, J.M., Seidman, L.J., Horton, N.J., Makris, N., Kennedy, D.N., Caviness Jr, V.S., Faraone, S.V., Tsuang, M.T., 2001. Normal sexual dimorphism of the adult human brain assessed by in vivo magnetic resonance imaging. *Cerebral Cortex* 11, 490–497.
- Green, S.A., Hernandez, L., Tottenham, N., Krasileva, K., Bookheimer, S.Y., Dapretto, M., 2015. Neurobiology of sensory overresponsivity in youth with autism spectrum disorders. *JAMA Psychiatry* 72, 778–786.
- Gürbüz, M.B., Rekik, I., 2021. Mgn-net: a multi-view graph normalizer for integrating heterogeneous biological network populations. *Medical Image Analysis* 71, 102059.
- Huang, Y., Chung, A.C., 2022. Disease prediction with edge-variational graph convolutional networks. *Medical Image Analysis* 77, 102375.
- Ji, J., Zhang, Y., 2022. Functional brain network classification based on deep graph hashing learning. *IEEE Transactions on Medical Imaging* 41, 2891–2902. doi:10.1109/TMI.2022.3173428.
- Jie, B., Zhang, D., Cheng, B., Shen, D., Initiative, A.D.N., 2015. Manifold regularized multitask feature learning for multimodality disease classification. *Human Brain Mapping* 36, 489–507.

- Kazi, A., Shekarforoush, S., Arvind Krishna, S., Burwinkel, H., Vivar, G., Kortüm, K., Ahmadi, S.A., Albarqouni, S., Navab, N., 2019a. Inceptioncn: receptive field aware graph convolutional network for disease prediction, in: International Conference on Medical Image Computing and Computer-assisted Intervention, Springer. pp. 73–85.
- Kazi, A., Shekarforoush, S., Arvind Krishna, S., Burwinkel, H., Vivar, G., Wiestler, B., Kortüm, K., Ahmadi, S.A., Albarqouni, S., Navab, N., 2019b. Graph convolution based attention model for personalized disease prediction, in: International Conference on Medical Image Computing and Computer-assisted Intervention, Springer. pp. 122–130.
- Kazi, A., Shekarforoush, S., Kortuem, K., Albarqouni, S., Navab, N., et al., 2019c. Self-attention equipped graph convolutions for disease prediction, in: 2019 IEEE 16th International Symposium on Biomedical Imaging, IEEE. pp. 1896–1899.
- Langen, M., Durston, S., Staal, W.G., Palmen, S.J., 2007. Caudate nucleus is enlarged in high-functioning medication-naive subjects with autism. *Biological Psychiatry* 62, 262–266.
- Li, Y., Zhang, X., Nie, J., Zhang, G., Fang, R., Xu, X., Wu, Z., Hu, D., Wang, L., Zhang, H., Lin, W., Li, G., 2022. Brain connectivity based graph convolutional networks and its application to infant age prediction. *IEEE Transactions on Medical Imaging* 41, 2764–2776. doi:10.1109/TMI.2022.3171778.
- Mohammadi-Nejad, A.R., Hossein-Zadeh, G.A., Soltanian-Zadeh, H., 2017. Structured and sparse canonical correlation analysis as a brain-wide multi-modal data fusion approach. *IEEE Transactions on Medical Imaging* 36, 1438–1448.
- Parisot, S., Ktena, S.I., Ferrante, E., Lee, M., Moreno, R.G., Glocker, B., Rueckert, D., 2017. Spectral graph convolutions for population-based disease prediction, in: International Conference on Medical Image Computing and Computer-assisted Intervention, Springer. pp. 177–185.
- Peng, P., Zhang, Y., Ju, Y., Wang, K., Li, G., Calhoun, V.D., Wang, Y.P., 2022. Group sparse joint non-negative matrix factorization on orthogonal subspace for multi-modal imaging genetics data analysis. *IEEE/ACM Transactions on Computational Biology and Bioinformatics* 19, 479–490. doi:10.1109/TCBB.2020.2999397.
- Ritter, K., Schumacher, J., Weygandt, M., Buchert, R., Allefeld, C., Haynes, J.D., 2015. Multimodal prediction of conversion to alzheimer’s disease based on incomplete biomarkers. *Alzheimer’s & Dementia: Diagnosis, Assessment & Disease Monitoring* 1, 206–215.
- Samson, F., Mottron, L., Soulières, I., Zeffiro, T.A., 2012. Enhanced visual functioning in autism: An ale meta-analysis. *Human Brain Mapping* 33, 1553–1581.
- Selvaraju, R.R., Cogswell, M., Das, A., Vedantam, R., Parikh, D., Batra, D., 2017. Grad-cam: Visual explanations from deep networks via gradient-based localization, in: Proceedings of the IEEE International Conference on Computer Vision, pp. 618–626.
- Song, X., Zhou, F., Frangi, A.F., Cao, J., Xiao, X., Lei, Y., Wang, T., Lei, B., 2022. Multi-center and multi-channel pooling gen for early ad diagnosis based on dual-modality fused brain network. *IEEE Transactions on Medical Imaging* .
- Stanfield, A.C., McIntosh, A.M., Spencer, M.D., Philip, R., Gaur, S., Lawrie, S.M., 2008. Towards a neuroanatomy of autism: a systematic review and meta-analysis of structural magnetic resonance imaging studies. *European Psychiatry* 23, 289–299.
- Su, C., Tong, J., Zhu, Y., Cui, P., Wang, F., 2020. Network embedding in biomedical data science. *Briefings in bioinformatics* 21, 182–197.
- Webb, S.J., Sparks, B.F., Friedman, S.D., Shaw, D.W., Giedd, J., Dawson, G., Dager, S.R., 2009. Cerebellar vermal volumes and behavioral correlates in children with autism spectrum disorder. *Psychiatry Research: Neuroimaging* 172, 61–67.
- Welling, M., Kipf, T.N., 2016. Semi-supervised classification with graph convolutional networks, in: International Conference on Learning Representations.
- Yamasaki, S., Yamasue, H., Abe, O., Suga, M., Yamada, H., Inoue, H., Kuwabara, H., Kawakubo, Y., Yahata, N., Aoki, S., et al., 2010. Reduced gray matter volume of pars opercularis is associated with impaired social communication in high-functioning autism spectrum disorders. *Biological Psychiatry* 68, 1141–1147.
- Zhang, H., Song, R., Wang, L., Zhang, L., Wang, D., Wang, C., Zhang, W., 2022a. Classification of brain disorders in rs-fmri via local-to-global graph neural networks. *IEEE Transactions on Medical Imaging* .
- Zhang, Y., Zhang, H., Xiao, L., Bai, Y., Calhoun, V.D., Wang, Y.P., 2022b. Multi-modal imaging genetics data fusion via a hypergraph-based manifold regularization: Application to schizophrenia study. *IEEE Transactions on Medical Imaging* 41, 2263–2272. doi:10.1109/TMI.2022.3161828.
- Zheng, S., Zhu, Z., Liu, Z., Guo, Z., Liu, Y., Yang, Y., Zhao, Y., 2022. Multi-modal graph learning for disease prediction. *IEEE Transactions on Medical Imaging* 41, 2207–2216. doi:10.1109/TMI.2022.3159264.
- Zhou, T., Liu, M., Thung, K.H., Shen, D., 2019. Latent representation learning for alzheimer’s disease diagnosis with incomplete multi-modality neuroimaging and genetic data. *IEEE Transactions on Medical Imaging* 38, 2411–2422.
- Zhu, Q., Wang, H., Xu, B., Zhang, Z., Shao, W., Zhang, D., 2022. Multi-modal triplet attention network for brain disease diagnosis. *IEEE Transactions on Medical Imaging* doi:10.1109/TMI.2022.3199032.